Reactions of Manganese and Rhenium Atoms with NO. Infrared Spectra and Density Functional Calculations of η^1 and η^2 Addition and Insertion Reaction Products

Lester Andrews* and Mingfei Zhou

Department of Chemistry, University of Virginia, Charlottesville, Virginia 22901

David W. Ball

Department of Chemistry, Cleveland State University, Cleveland, Ohio 44115

Received: July 31, 1998; In Final Form: October 9, 1998

Reactions of thermal and laser-ablated Mn atoms with NO produce the Mn−(η^1-NO)$_x$ complexes ($x = 1-3$), a series of η^2 complexes, and in addition, laser-ablated Mn gives the NMnO insertion product. The C_{2v} complex $Mn(NO)_2$ is identified from symmetric (a_1) and antisymmetric (b_2) N−O ligand stretching modes, which gave triplet mixed isotopic spectra and excellent agreement with DFT calculations. The $Mn(NO)_3$ complex is shown to have C_{3v} symmetry through the observation of mixed isotopic spectra for four vibrational modes, including the symmetric (a_1) and antisymmetric (e) N−O ligand stretching modes and a match with DFT calculations of isotopic frequencies. Laser-ablated Re gave similar major products.

Introduction

The nitric oxide molecule is very similar to carbon monoxide in forming complexes with transition-metal atoms; however, NO has an additional antibonding π electron for coordination, and nitrosyl chemistry is much less extensive than carbonyl chemistry.[1] Although only one pure nitrosyl, $Cr(NO)_4$, has been characterized as the neat material,[2,3] matrix isolation studies of thermal Fe, Co, Ni, and Cu reactions with NO have provided evidence for several small nitrosyl species,[4−6] and a recent laser-ablation study with Cr has produced Cr−(η^1-NO)$_x$ ($x = 1-4$), Cr-η^2-NO, and the stable NCrO insertion product.[7] A detailed density functional study of first-row transition-metal nitrosyls should provide a guide for interpreting experimental spectra.[8] Here follows a comparison of thermal Mn atom reactions and laser-ablated Mn and Re atom reactions with NO and of density functional calculations for MnNO isomers, $Mn(NO)_2$, and $Mn(NO)_3$.

Experimental Section

The apparatus and technique for reactions of laser-ablated metal atoms with small molecules during condensation in excess argon has been described in a number of reports from this laboratory.[9−12] Manganese (Johnson Matthey) and rhenium (Goodfellow) metal targets were mounted on a rotating rod and ablated by a focused YAG laser and co-deposited with isotopic nitric oxide samples onto a 10−11 K substrate for 1 h as described previously.[9−14] FTIR spectra were recorded at 0.5 cm^{-1} resolution on a Nicolet 750 using an MCTB detector after sample deposition, after annealing, and after broad-band photolysis.

Details of the vacuum system used for thermal metal-atom experiments have been presented previously.[4−6,15] Manganese metal was placed in an alumina crucible, which was heated in a tantalum foil tube furnace to 900−1100 °C. The deposition rate was monitored with a quartz crystal microbalance (Inficon). Vapors were condensed onto one face of a gold-plated, octagonal copper block attached to the cold stage of an APD Displex closed-cycle helium refrigerator; the block temperature was 12−14 K. Depositions lasted for 15 min, and after deposition, the reflection FTIR spectrum was measured with a Nicolet 5-DX Fourier transform infrared spectrometer at 2 cm^{-1} resolution.

Results

Experimental spectra will be presented for Mn and Re reactions with NO.

Laser-Ablated Mn. Experiments were done with medium, low, and threshold laser energies[9−12] and normal isotopic NO at 0.4%, 0.2% and 0.1% concentrations in excess argon. New product absorptions are listed in Table 1; bands common to other metal reactions with NO including N_2O, NO_2, $(NO)_2^+$, NO_2^-, *cis*- and *trans*-$(NO)_2^-$ are omitted.[7,13−17] Figures 1 and 2 illustrate the spectrum with the 0.1% NO sample and low laser energy; note only the very weak 1693.0 cm^{-1} product band above 1000 cm^{-1} and very weak product bands at 948.0 (OMnO),[12] 932.3 and 874.0, 833.3 (MnO),[12] and 451.7 cm^{-1} on sample deposition (traces a). Broad-band photolysis increased the 932.3 and 874.0 cm^{-1} band pair (times 4), produced a very weak 987.8 cm^{-1} band, and decreased the 451.7 cm^{-1} band without other effects (traces b). Stepwise annealing was done to 25, 30, 35, and 40 K, and the first three of these are shown in Figures 1 and 2. Note the increase of $(NO)_2$ and the appearance of a weak 1748.6 cm^{-1} band, stronger bands at 1713.2 and 1693.0 cm^{-1}, and weak bands at 1662.6, 1268.7, 1236.8, 1232.4, 994.1, 838.8, 594.2, 534.3, and 456.2 cm^{-1} on first annealing (trace c). The 932.3 and 874.0 cm^{-1} band pair increased 1.25 times the OMnO and MnO absorptions, and the 451.7 cm^{-1} band also increased considerably. The second annealing increased most of the absorptions but decreased the 932.3, 874.0 cm^{-1} pair, and the third annealing continued this trend (traces d, e). A final annealing to 40 K (not shown) slightly increased the 994.1, 838.8 cm^{-1} set, decreased the 932.3, 874.0 cm^{-1} pair, increased the 1713.2, 534.3 cm^{-1} bands by 20%, and decreased the 1693.0 cm^{-1} band by 10%.

10.1021/jp983235u CCC: $15.00
Published on Web 11/14/1998

TABLE 1: Infrared Absorptions (cm^{-1}) from Co-Deposition of Laser-Ablated Manganese Atoms with NO in Excess Argon at 10 K

$^{14}N^{16}O$	$^{15}N^{16}O$	$^{15}N^{18}O$	$^{14}N^{16}O + {}^{15}N^{16}O$	R(14/15)	R(16/18)	assignment
1843.4	1806.8	1764.4	1843.5, 1806.8	1.02025	1.02403	$(ON)MnO_2$
1827.0[a]	1790.9	1750.1	1816.9, 1808.3, 1790.0	1.02016	1.02331	$Mn_x(NO)_y$
1824.1	1788.0	1747.2	1824.1, 1814.3, 1802.7, 1788.0	1.02014	1.02335	$Mn(NO)_3$
1794.8	1761.0	1720.7		1.10919	1.02342	(ON)MnO
1791.5	1757.6	1717.4		1.01929	1.02341	(ON)MnO
1766 sh	1731 sh	1691 sh				$Mn(NO)_x(NO^*)$
1748.6	1713.3	1675.9		1.02060	1.02232	(MnNO)
1747.2	1713.3	1673.7		1.01979	1.02366	$Mn_x(NO)_y$
1744.7	1709.8	1670.8	1744.7, 1732.6, 1709.8	1.02041	1.02334	$Mn(NO)_2$
1737.3	1703.4		1737.3, 1703.1	1.01990		$Mn(NO)_x(NO^*)$
1728.0	1694.2	1654.9	1728, 1720, 1706, 1694	1.01995	1.02375	$Mn_x(NO)_y$
1713.2	1679.8	1640.6	1713.2, 1699.2, 1688.8, 1679.8	1.01988	1.02389	$Mn(NO)_3$
1693.0	1659.1	1622.4	1693.1, 1670.8, 1659.0	1.02043	1.02262	$Mn(NO)_2$
1675.1	1645.0	1601.3		1.01830	1.02729	aggregate
1662.6	1629.3	1593.3	1662.6, 1639.6, 1629.3	1.02044	1.02259	$(Mn_2(NO)_2)$
1487.1	1461.4	1423.3	1463.6, 1461.8	1.01759	1.02677	$Mn(NO)_x(NO^*)$
1363.6	1337.2	1305.3	1363.4, 1337.3	1.01974	1.02444	$Mn(NO)_x(NO^*)$
1268.7	1249.0	1218.7	1268.7, 1253.2, 1249.0	1.01577	1.02486	$Mn[NO]_2$
1236.8	1213.8	1181.0	1236.8, 1213.8	1.01895	1.02777	Mn[NO]
1232.4	1216.1	1175.2	1232.4, 1216	1.01340	1.03480	Mn[NO] F. R.
1216.5	1189.5	1159.2		1.02270	1.02614	X−Mn[NO]
1002.8	974.7	973.4		1.02883	1.00134	(NMnMnO) site
994.1	965.0	964.9	994.2, 965.0	1.03016	1.00010	(NMnMnO)
987.8	987.8	951.0	987.8, 974.2, 951.0	1.00000	1.03870	$(ON)MnO_2$
979.8	979.7	943.3			1.03859	$(ON)_xMnO_2$
948.0	948.0	912.5			1.03890	OMnO
932.3	918.7	906.2	932.3, 918.6	1.01480	1.01379	NMnO
918.4	911.6	891.5		1.00746	1.02255	aggregate
874.0	863.5	837.6	874.0, 863.5	1.01216	1.03092	NMnO
862.3	861.5	821.5	861.9	1.00093	1.04869	(ON)MnO
858.3	858.0	818.2	858.1	1.00035	1.04864	(ON)MnO
838.8	838.8	797.5			1.05179	(NMnMnO)
833.1	833.1	796.7			1.04581	MnO
737.2	724.3			1.01781		
695.5	693.5	668.7		1.00288	1.03709	aggregate
614.0	610.3	587.8	613.8, 613.1, 610.4, 609.7	1.00606	1.03828	aggregate
599.2	593.7	584.1		1.00926	1.01644	aggregate
594.1	590.0	577.8	594.1, 592.1, 590.0	1.00695	1.02111	$Mn(NO)_3$
591.0	587.0	574.9		1.00681	1.02105	$Mn(NO)_3$
539.3	524.8	520.2		1.02763	1.00884	$Mn(NO)_3$ site
534.3	519.7	515.2	534.3,532.8, 528.0, 526.4, 521.5, 519.7	1.02809	1.00873	$Mn(NO)_3$
456.2	452.4	441.9	456.2, 454.1. 452	1.00840	1.02376	site
451.7	447.2	437.6	451.7, 447.2	1.01006	1.02194	Mn[NO]Mn

[a] Italic bands also observed in thermal Mn atom experiments.

The use of higher NO concentration at threshold laser energy favored the 1713.2, 534.3 cm^{-1} bands over the 1693.0 cm^{-1} band and associated new bands at 1824.0 and 1744.7 cm^{-1}, respectively, and favored the 1713.2, 1824.1 cm^{-1} pair relative to the 1827.0, 1728.8 cm^{-1} pair. Experiments with higher laser energy relative to NO concentration favored the 994.1, 838.8 cm^{-1} set relative to the 932.3, 874.0 cm^{-1} pair.

Isotopic experiments were performed with 0.2% ^{15}NO, 0.3% ($^{14}NO + {}^{15}NO$, 1:1), and 0.2% ($^{15}N^{16}O + {}^{15}N^{18}O$, 1:3), and isotopic band positions are listed in Table 1. Isotopic multiplets are also listed for the $^{14}NO + {}^{15}NO$ mixture, and selected spectra are shown in Figures 3 and 4.

Thermally Evaporated Mn. Experiments were done by varying the Mn concentration from <0.1% to >1% at a constant NO concentration of 0.2%, and spectra are shown in Figure 5. The 1693 cm^{-1} band and a very weak 1713 cm^{-1} absorption are observed in the lowest Mn concentration deposit <0.1%, Figure 5a. Successively higher Mn concentrations produce stronger bands and reveal weaker 1748 and 1744 cm^{-1} features (traces b−d). The final deposit, at the highest Mn concentration, >1%, scan e, gives still stronger bands and new absorptions at 1827 and 1728 cm^{-1} and at 1487, 1268, 1237, and 1232 cm^{-1}. A similar study with 0.8% Mn and <0.1%, 0.2%, 0.3%, and 0.5% NO is dominated by the 1693 cm^{-1} band, but the 1713 cm^{-1} band increases relative to the 1693 cm^{-1} band with increasing NO concentration, and the weaker 1827 and 1728 cm^{-1} bands follow this trend.

Laser-Ablated Re. A series of experiments was done with laser-ablated Re atoms and isotopic NO molecules, and the product absorptions are listed in Table 2. Figure 6 shows a composite spectrum contrasting the three isotopic samples. In the upper region, very weak bands were observed at 1677.7 and 1651.6 cm^{-1} on deposition with ^{14}NO and at 1117.2, 1052.9, 933.1, 907.3, 903.2, and 901.2 cm^{-1} in the lower region, trace a. Annealing to 25 K, scan b, markedly increased the 1677.7 and 1651.6 cm^{-1} bands, produced a weak new 1137.0 cm^{-1} band, decreased the 1117.2 cm^{-1} feature, increased the 1052.9 cm^{-1} band and 1054.7 cm^{-1} satellite and the 903.2, 901.2 cm^{-1} bands, and produced new features near 880 cm^{-1}. Scans c and d illustrate the same spectra for $^{15}N^{16}O$, while traces e and f do likewise for $^{15}N^{18}O$. Note large shifts in the upper region for both substitutions, but in the lower region, some bands depend more on nitrogen and others on oxygen isotopic substitution.

Calculations

Density functional theory calculations were performed on all the MnNO isomers using the Gaussian 94 program.[18] The BP86 functional[19,20] and 6-311+G* basis sets[21,22] were used for N and O, and the Wachters/Hay set as modified by Gaussian 94

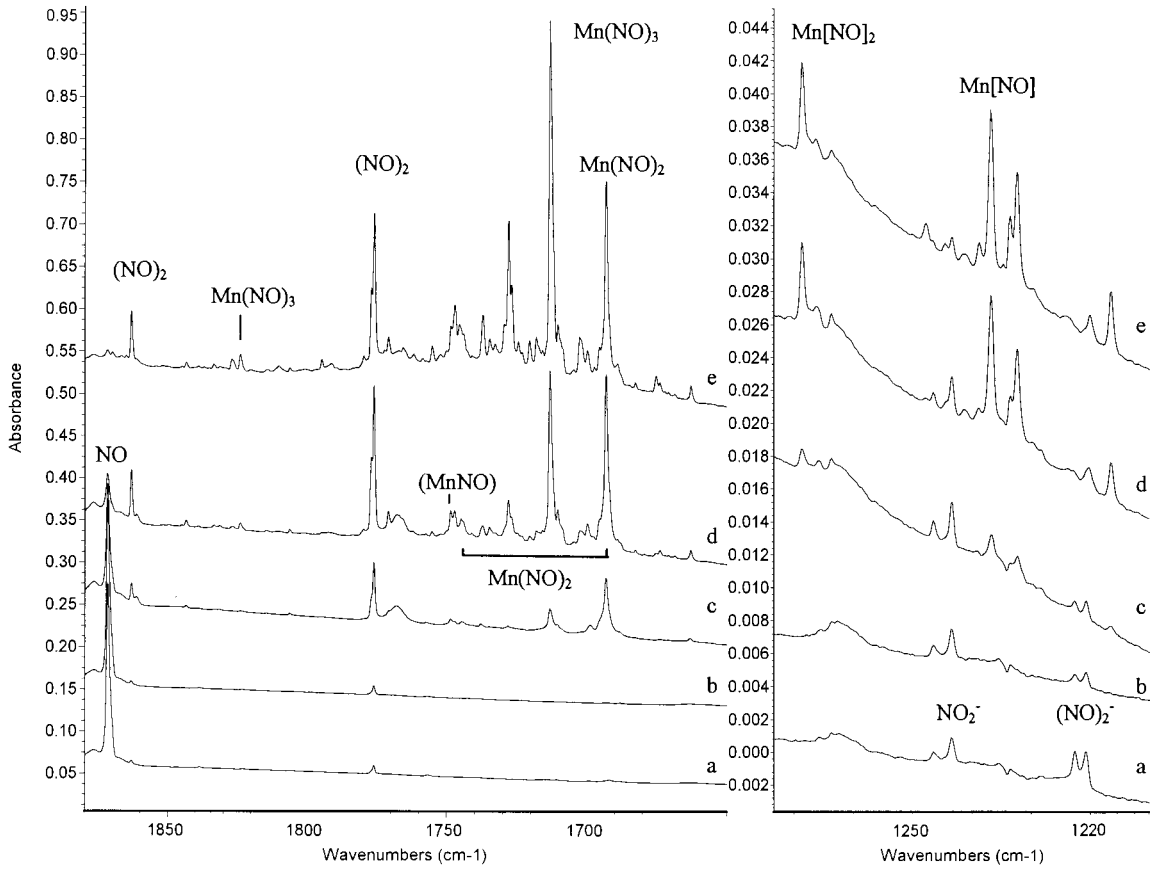

Figure 1. Infrared spectra in the 1880−1650 and 1275−1210 cm^{-1} regions for products of the reaction of laser-ablated Mn atoms with NO (0.1%) in excess argon during condensation at 10 K: (a) spectrum of deposited sample, (b) after broad-band photolysis for 20 min, (c) after annealing to 25 K, (d) after annealing to 30 K, and (e) after annealing to 35 K.

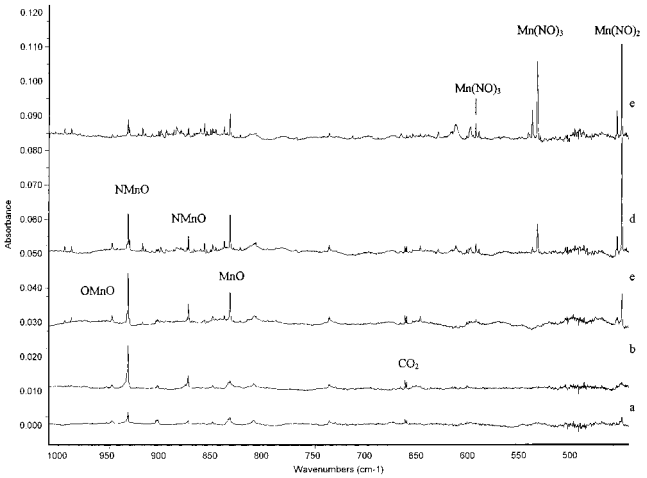

Figure 2. Infrared spectra in the 1010−440 cm^{-1} region for products of the reaction of laser-ablated Mn atoms with NO (0.1%) in excess argon during condensation at 10 K: (a) spectrum of deposited sample, (b) after broad-band photolysis for 20 min, (c) after annealing to 25 K, (d) after annealing to 30 K, and (e) after annealing to 35 K.

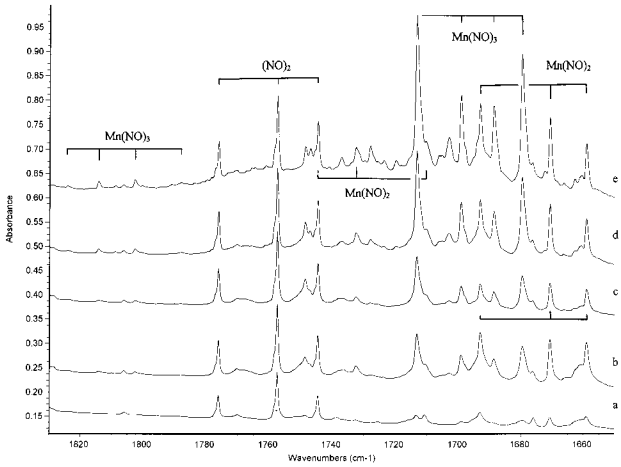

Figure 3. Infrared spectra in the 1830−1650 cm^{-1} region for the reaction of laser-ablated Mn atoms with ^{14}NO + ^{15}NO (0.3%, 1:1) in excess argon during condensation at 10 K: (a) spectrum of deposited sample, (b) after annealing to 25 K, (c) after broad-band photolysis for 20 min, (d) after annealing to 30 K, and (e) after annealing to 35 K.

was used for Mn.[23] Previous work has shown that the BP86 functional works well for transition-metal systems, particularly for frequency calculations.[11,24−28] The geometries and relative energies calculated for the MnNO, MnON, NMnO, and cyclic Mn[NO] isomers in low-lying states are listed in Table 3, and the isotopic frequencies, intensities, and isotopic frequency ratios are listed in Table 4. These calculations are considered as a first approximation and as a guide for vibrational assignments. For the NMnO molecule, the ground state is ^{3}A″ and the ^{5}A″ state is 24.8 kcal/mol higher in energy. For MnNO, also known as Mn−(η^1-NO), the calculated ground state is ^{5}A″ and the $^3\Sigma^-$ state is 2.9 kcal/mol higher. For cyclic Mn[NO], also known as Mn−(η^2-NO), the ground state is ^{3}A″ and the MnON $^3\Sigma^-$ state is 20.4 kcal/mol higher. Triplet NMnO is the global minimum at this level of theory, and triplet MnNO, Mn[NO], and MnON are 7.1, 19.8, and 40.2 kcal/mol higher in energy. Calculations were also done for triplet NMnO using the B3LYP functional, and the results are footnoted in the tables. Similar calculations

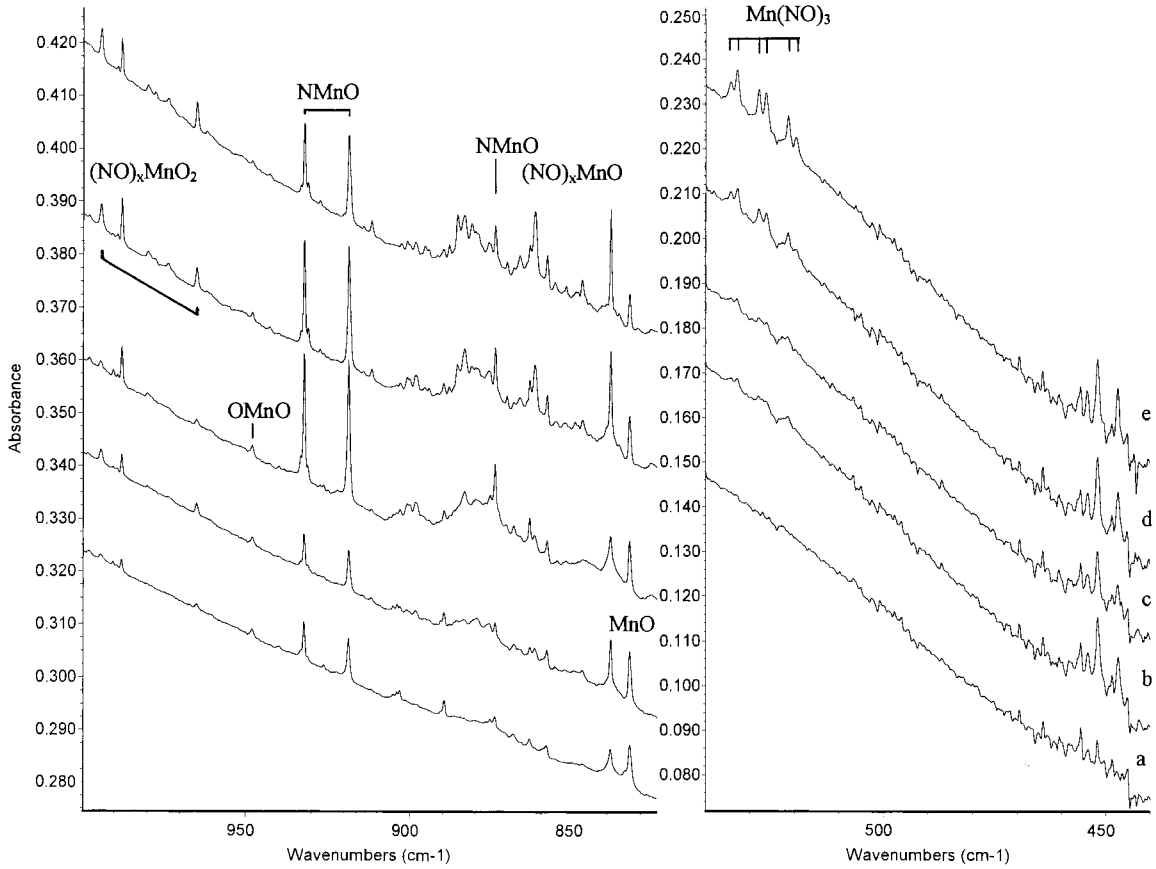

Figure 4. Infrared spectra in the 1000−825 and 540−440 cm^{-1} regions for the reaction of laser-ablated Mn atoms with $^{14}NO + {}^{15}NO$ (0.3%, 1:1) in excess argon during condensation at 10 K: (a) spectrum of deposited sample, (b) after annealing to 25 K, (c) after broad-band photolysis for 20 min, (d) after annealing to 30 K, and (e) after annealing to 35 K.

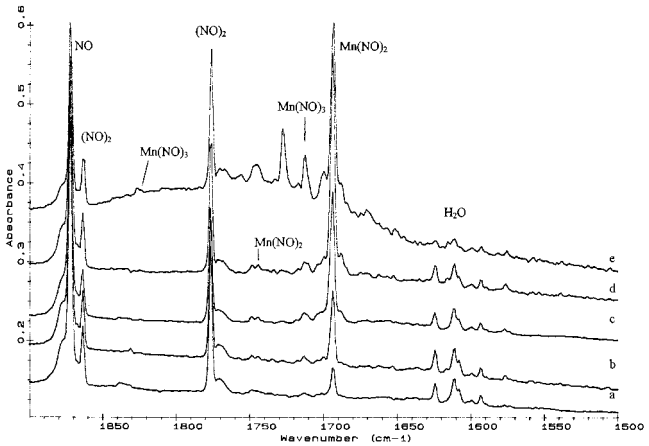

Figure 5. Infrared spectra in the 1900−1500 cm^{-1} region for thermal Mn atoms at different concentrations co-deposited with NO (0.2%) in excess argon at 13 ± 1 K: (a) less than 0.1% Mn, (b) 0.2% Mn, (c) 0.3% Mn, (d) 0.6% Mn, and (e) greater than 1% Mn in argon.

were also done for the anions $NMnO^-$ and $MnNO^-$, and the results are also listed in Tables 3 and 4.

Calculations were first done for $Mn(NO)_2$ using a smaller 6-311G* basis set. A $^2A_1$ molecule was calculated with 1.633 and 1.188 Å bond distances for Mn−N and N−O, respectively, and 166.3° and 103.6° for Mn−N−O and N−Mn−N angles. The calculation was repeated with the larger 6-311+G* basis set. The results are presented in Table 5; the nitrosyl stretching frequencies decreased 17 and 27 cm^{-1} with the larger basis set. The $^4A_1$ state is 14.0 kcal/mol higher in energy and has Mn−N = 1.731 Å, N−O = 1.191 Å, ∠N−Mn−N = 155.5° and has similar nitrosyl frequencies (1762.3, 1685.7 cm^{-1}). A similar calculation for $Mn(NO)_2^-$ found a $^1A_1$ ground state with Mn−N = 1.632 Å, N−O = 1.222 Å, ∠N−Mn−N = 114.5°. The N−O stretching frequencies are 1626.5 (a_1, 747 km/mol) and 1573.7 cm^{-1} (b_2, 1084 km/mol). The anion energy is lower by 42.3 kcal/mol, a reasonable amount for the electron affinity of $Mn(NO)_2$.

The same procedure was followed for $Mn(NO)_3$, and the results for the 6-311G* basis calculation are given in Table 6 for isotopic and mixed isotopic frequencies in the $^1A''$ state. The 6-311+G* basis gave N−O stretching frequencies 15 and 4 cm^{-1} lower, Mn−N mode 6 cm^{-1} lower, and Mn−N = 1.684 Å, N−O = 1.179 Å, ∠Mn−N−O = 164.5°, ∠N−Mn−N = 108.5°. Structures calculated for the major reaction products are shown in Figure 7.

Discussion

The new product bands will be identified and assigned with the help of reagent concentration variation, isotopic substitution, and DFT vibrational frequency calculations.

NMnO. In previous Mn + O_2 experiments, the manganese dioxide molecule ($\nu_3 = 948$ cm^{-1}, $\nu_1 = 816$ cm^{-1}) was produced by insertion of Mn into O_2 while in N_2 investigations a possible NMnN molecule ($\nu_3 = 859$ cm^{-1}) was formed by reaction of N atoms with MnN molecules.[11,12] One goal of this work is to determine if Mn can undergo the insertion reaction with NO. Sharp bands were observed in the laser-ablation experiments at 932.3 and 874.0 cm^{-1}; these bands increased together on photolysis and first annealing and decreased together on subsequent annealing cycles (Figure 1). The two bands were barely detected with threshold laser power, but strong bands

TABLE 2: Infrared Absorptions (cm^{-1}) from Co-Deposition of Laser-Ablated Rhenium Atoms with NO in Excess Argon at 10 K

$^{14}N^{16}O$	$^{15}N^{16}O$	$^{15}N^{18}O$	$^{14}N^{16}O + {}^{15}N^{16}O$	R (14/15	R (16/18)	assignment
2122.8	2052.3		2122.8, 2080, 2052.3	1.03435		(N_2)NReO
2109.7	2039.9	2039.9	2075.3	1.0342		(N_2)NReO
2104.7	2034.9	2034.9	2070.2	1.03435		(N_2)NReO
1871.8	1838.9	1789.3	1871.8, 1838.8	1.01789	1.02778	NO
1749.3	1719.1	1679.0		1.01757	1.02388	aggregate
1728.8	1692.3	1662.1		1.02157	1.01817	aggregate
1702.0	1668.9	1629.9		1.01983	1.02393	aggregate
1688.0	1660.4			1.01662		N_2O_3
1684.2	1650.8	1613.3		1.02023	1.02324	$Re_x(NO)_y$
1677.7	1645.1	1606.6		1.01982	1.02396	$Re(NO)_3$
1651.6	1622.4	1579.2	1651.5, 1634.3, 1622.4	1.01800	1.02736	$Re(NO)_2$
1630.0	1593.9	1564.3		1.02265	1.01892	N_2O_3
1610.8	1576.3	1545.7		1.02189	1.01980	NO_2
1589.4	1562.0	1520.4		1.01754	1.02736	$(NO)_2^+$
1583.4	1556.3	1514.9		1.01741	1.02733	$(NO)_2^+$
1144.8	1124.9			1.01769		Re[NO] site
1137.0	1117.4	1087.3	1137.0, 1117.4	1.01754	1.02768	Re[NO]
1117.2	1082.3	1082.3		1.03225		ReN
1068.2	1048.5	1023.1		1.01879	1.02483	
1054.7	1024.0	1020.7	1054.7, 1024.0	1.02998	1.00323	NReO
1052.9	1022.2	1019.1	1053.0, 1022.3	1.03003	1.00304	NReO
1043.9	1013.4	1009.1		1.03010	1.00426	NReO(NO)
1038.0	1007.2	1004.9		1.03058	1.00229	$NReO^-$
933.1	933.1	886.7	933.1	1.000	1.05233	OReO
930.3	930.3	884.0	930.3	1.000	1.05142	(N_2)OReO
924.8	924.7	878.8	924.8	1.000	1.05223	complex
903.2	901.5	857.5	903.3, 901.4	1.00189	1.05131	NReO
901.2	899.5	855.5	901.4, 899.5	1.00185	1.05143	NReO
891.7	889.9	847.1		1.00202	1.05051	NReO(NO)
888.4	885.8	843.9	sum	1.00294	1.04965	(N_2)OReO
886.8	884.3	842.1	sum	1.00269	1.05027	(N_2)OReO
880.2	878.4	835.4	880.2, 878.3	1.00194	1.05159	(N_2)NReO
874.0	872.3	829.7	874.0, 872.4	1.00206	1.05122	(N_2)NReO
860.9	859.5	819.0		1.00154	1.04953	$NReO^-$

TABLE 3: Relative Energies and Structures Calculated (BP86/6-311+G*) for MnNO Isomer States

molecule	state	relative energies (kcal/mol)	geometry (Å, deg)
NMnO[a]	$^3A''$	0	MnN,1.5503; MnO,1.6188; ∠NMnO,117.0°
MnNO[b]	$^5A''$	+4.2	MnN,1.7506; NO,1.2020; ∠MnNO,149.6°
MnNO[b]	$^3\Sigma^-$	+7.1	MnN,1.6370; NO,1.1903; ∠MnNO, 180°
Mn[NO][c,d]	$^3A''$	+19.8	MnN,1.7524; MnO,1.9513; NO,1.2753
NMnO	$^5A''$	+24.8	MnN,1.6372; MnO,1.6113; ∠NMnO,125.3°
NMnO	$^1A'$	+25.2	MnN,1.5322; MnO,1.6152; ∠NMnO,121.6°
MnON[e]	$^3\Sigma^-$	+40.2	MnO,1.7634; ON,1.2232; ∠MnON, 180°
$MnNO^-$	$^4A''$	−24.5	MnN,1.7114; NO,1.2264; ∠MnNO,155.7°
$NMnO^-$	$^2A''$	−44.6	MnN,1.5677; MnO,1.6446; ∠NMnO,121.1°
$NMnO^-$	$^4A''$	−56.4	MnN,1.5835; MnO,1.6599; ∠NMnO,127.4°

[a] The B3LYP functional gave MnN, 1.5835; MnO, 1.6172; ∠NMnO, 121.3°. [b] Also known as Mn−(η^1-NO), the end-bonded nitrosyl. [c] Also known as Mn−(η^2-NO), the side-bonded cyclic species. [d] Mn[NO] quintet converged to MnNO. [e] MnON quintet converged to MnNO.

with the same 3:1 relative intensity were produced on broad-band photolysis. Deposition with the highest laser power gave the two bands with absorbances much like the spectrum in Figure 1c. These bands were not observed with thermal Mn atoms.

Mixed isotopic spectra reveal doublets that are the sum of pure isotopic spectra for each band (Figure 4). This shows that one N and one O atom are involved in each vibrational mode and suggests that the 932.3 and 874.0 cm^{-1} bands are due to the NMnO insertion product as these bands are near recent argon matrix absorptions for MnN (916.1 cm^{-1}) and MnO (833.1 cm^{-1}).[11,12]

This assignment receives only limited support from BP86/6-311+G* calculations of the $^3A''$ bent NMnO ground state in the general positions of the two terminal-bond stretching frequencies at 1026.8 (Mn−N) and 932.4 cm^{-1} (Mn−O) but not in the nature of the mixed stretching coordinates, as determined by isotopic ratios. The B3LYP functional gives even poorer agreement: 950.6 (Mn−O) and 637.4 cm^{-1} (Mn−N) frequencies that are almost pure Mn−O and Mn−N stretching modes, respectively. Note that both functionals predict nearly the same Mn−O mode just above the observed 874.0 cm^{-1} band, which is mostly Mn−O stretching, but the functionals differ by almost 300 cm^{-1} in predicting the Mn−N stretching mode. Apparently several low-lying d-orbital configurations are mixing in the $^3A''$ state to give normal modes that are mixtures of the Mn−N and Mn−O internal bond-stretching coordinates. A higher level multiconfiguration calculation will have to be performed to explain the normal mode structure of bent NMnO.

Mn[NO] or Mn−(η^2-NO). The complex Cr−(η^2-NO) has been characterized by a strong N−O stretching mode at 1108.8 cm^{-1}, with isotopic ratios just under diatomic values, and DFT calculations of this side-bonded species.[7] At progressively higher frequencies, 1132.2 and 1448.8 cm^{-1} absorptions show evidence

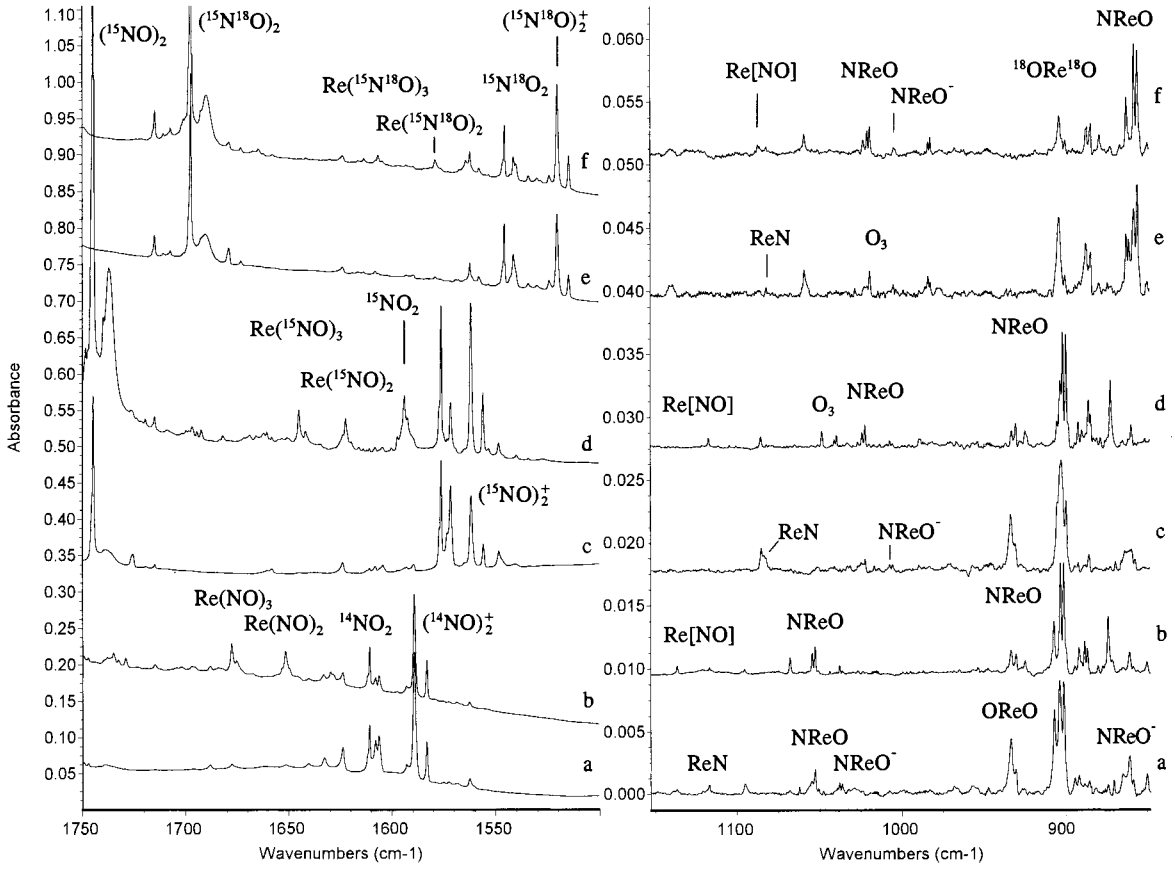

Figure 6. Infrared spectra in the 1750−1500 and 1150−850 cm^{-1} regions for laser-ablated Re atoms co-deposited with isotopic nitric oxide samples (0.3%) in excess argon at 10 K: (a) $^{14}N^{16}O$-deposited sample, (b) after annealing to 25 K, (c) $^{15}N^{16}O$ deposited sample, (d) after annealing to 25 K, (e) $^{15}N^{18}O$ deposited sample, and (f) after annealing to 25 K.

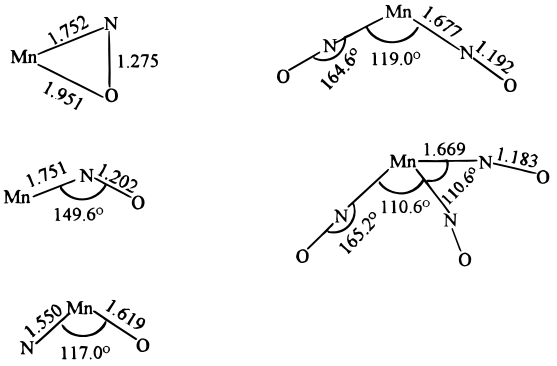

Figure 7. Structures calculated by DFT (BP86/6-311+G*) for major reaction products. Bond distances given in angstroms.

of isotopic mixing and the attachment of η^1-nitrosyl ligands to the Cr−(η^2-NO) complex. These complexes are photosensitive, ultimately giving way to the most stable Cr−(η^1-NO)$_4$ complex. The spectra of V and Fe with NO, currently under investigation, also have absorptions with similar isotopic characteristics in this region. The 1236.8, 1232.4 cm^{-1} doublet grows in on annealing (Figure 1), and it appears on deposition with higher laser power and grows further on annealing and on photolysis. These bands show isotopic shifts with $^{15}N^{16}O$ and $^{15}N^{18}O$ and mixed isotopic spectra that are the sum of pure isotopic spectra. Hence, a single NO molecule is involved in these vibrations. Studies with Cr showed that the 1200 cm^{-1} region is appropriate for sideways bonded (-η^2-) NO species, so Mn[NO] must be considered. The $^3A''$ ground-state calculation predicts a strong band at 1261.5 cm^{-1} and isotopic ratios (1.0173, 1.0292) in reasonable agreement with the observed values for the strong 1236.8 cm^{-1} band (see Tables 1 and 4). The best explanation for the 1232.4 cm^{-1} band is the overtone of the unobserved Mn−N stretching fundamental calculated at 591.3 cm^{-1} in Fermi resonance with the 1236.8 cm^{-1} band. In such an event, the calculation has slightly underestimated this fundamental frequency. In the $^{15}N^{16}O$ case, the overtone red shifts about 30 cm^{-1} and the fundamental only 21 cm^{-1} so the interaction is diminished and a weak 1216.1 cm^{-1} overtone results. In the $^{15}N^{18}O$ case, the N−O fundamental is now below the overtone and the interaction remains weak.

Mn[NO]$_2$. The 1268.7 cm^{-1} band also grew on annealing and exhibited a sharp 1:2:1 triplet at 1268.7, 1253.2, 1249.0 cm^{-1}, suggesting that two equivalent NO submolecules participate in this vibration. On this basis, the 1268.7 cm^{-1} band is assigned to the bicyclic Mn[NO]$_2$ species.

MnNO or Mn−(η^1-NO). The present and earlier[8] DFT calculations predict the $^5A''$ MnNO complex slightly below the $^3\Sigma^-$ state and a strong N−O vibrational mode near 1600 cm^{-1} for the quintet or 1740 cm^{-1} for the triplet. We observe no possible assignment for MnNO in the 1600 cm^{-1} region, but the 1748.6 cm^{-1} band *might be* due to MnNO. The observed 14/15 and 16/18 isotopic ratios are in reasonable agreement with the calculated values. The 1748.6 cm^{-1} band appears on 25 K annealing in the dilute reagent experiment (Figure 1), increases on annealing to 30 K, and decreases thereafter, and this band is observed on deposition with higher reagent concentrations. Unfortunately, band congestion makes it impossible to characterize the mixed isotopic spectrum, so this possible identification of MnNO is tentative.

Mn(NO)$_2$ or Mn−(η^1-NO)$_2$. The much stronger 1693.0 cm^{-1} band is easier to characterize; it increases markedly on early

TABLE 4: Isotopic Frequencies (cm^{-1}), Intensities (km/mol), and Ratios Calculated (BP86/6-311+G*) for the Structures Described in Table 3

	14−16, ν (I)	15−16, ν (I)	15−18, ν (I)	R(14−16/15−16)	R(15−16/15−18)
NMnO	328.2(1)[a]	323.4(1)[b]	316.5(1)[b]	1.0148	1.0218
(^{3}A″)	932.4(121)	932.1(116)	891.4(108)	1.0003	1.0457
	1026.8(61)	999.5(63)	999.5(62)	1.0273	1.0000
MnNO	228.6(31)	224.5(30)	219.7(29)	1.0183	1.0219
(^{5}A″)	517.0(20)	508.8(18)	501.4(19)	1.0162	1.0148
	1638.3(655)	1607.2(631)	1566.5(599)	1.0194	1.0260
MnNO	298.6(7)	291.0(7)	287.4(7)	1.0261	1.0125
($^3\Sigma^-$)	583.1(11)	578.6(11)	564.4(10)	1.0078	1.0252
	1742.5(954)	1706.8(910)	1668.3(879)	1.0209	1.0231
Mn[NO]	288.0(8)	286.8(8)	275.4(7)	1.0042	1.0414
(^{3}A″)	591.3(13)	576.3(12)	575.5(12)	1.0260	1.0014
	1261.5(242)	1240.0(233)	1204.8(221)	1.0173	1.0292
NMnO	203.5(18)	201.0(17)	196.5(16)	1.0124	1.0229
(^{5}A″)	758.7(27)	743.0(27)	737.7(25)	1.0211	1.0072
	884.5(75)	878.6(73)	845.1(70)	1.0067	1.0396
NMnO	355.6(5)	350.4(5)	343.2(5)	1.0148	1.0210
(^{1}A′)	930.8(144)	930.7(141)	889.9(129)	1.0001	1.0459
	1098.7(107)	1069.3(104)	1069.3(106)	1.0275	1.0000
MnON	136.0(0.4)	134.5(0.4)	129.4(0.3)	1.0112	1.0394
($^3\Sigma^-$)	460.9(0.1)	454.9(0.1)	447.8(0.1)	1.0132	1.0159
	1468.9(235.8)	1446.1(228)	1401.0(215)	1.0158	1.0322
MnNO$^-$	207.1(23)	202.5(22)	199.1(21)	1.0227	1.0171
(^{4}A″)	485.7(4)	480.0(3)	470.9(4)	1.0119	1.0193
	1518.5(957)	1488.9(924)	1452.5(874)	1.0199	1.0251
NMnO$^-$	290.4(0.2)	286.4(0.2)	280.4(0.1)	1.0140	1.0214
(^{4}A″)	855.0(161)	853.5(152)	816.7(143)	1.0018	1.0451
	997.5(225)	972.3(223)	971.5(212)	1.0259	1.0008
NMnO$^-$	303.6(0)	299.2(0)	292.9(0)	1.0147	1.0215
(^{2}A″)	879.9(182)	879.8(180)	841.4(160)	1.0001	1.0456
	1042.9(174)	1015.1(165)	1015.1(167)	1.0274	1.0000

[a] The B3LYP functional gave 265.4(15), 638.7(17), and 950.6(185). [b] The B3LYP functional gave 261.9, 621.3, 950.5 cm^{-1} for 15−16 and 256.3, 620.8, 909.3 cm^{-1} for 15−18.

TABLE 5: Isotopic Frequencies (cm^{-1}) and Intensities (km/mol) Calculated (BP86/6-311+G*) for Mn(NO)$_2$ in the ^{2}A$_1$ State[a]

(14−16)$_2$, ν (I)	(15−16)$_2$	(15−18)$_2$
1762.3(188)	1726.1	1687.2
1696.9(1238)	1662.5	1624.4
634.7(6)	623.3	616.0
625.2(1)	620.2	608.1
548.0(0.2)	537.5	526.7
372.0(27)	362.6	359.3
294.4(0)	287.0	282.8
289.4(6)	282.5	277.7
73.4(2)	73.3	70.0

[a] Structure: C_{2v} symmetry, Mn−N = 1.677 Å, N−O = 1.192 Å, ∠Mn−N−O = 164.6°, ∠N−Mn−N = 119.0°.

annealing and decreases on final annealing while the 1713.2 cm^{-1} band still increases. The mixed ^{14}NO + ^{15}NO isotopic spectrum shows a clear 1:2:1 triplet at 1693.1, 1670.6, 1659.0 cm^{-1}, and the ^{15}N^{18}O experiment shows an intermediate component at 1634.5 cm^{-1} owing to ^{15}N^{16}O present in the sample. The 1693.0 cm^{-1} band is due to the vibration of two equivalent NO submolecules. The 14−16/15−16 and 15−16/15−18 isotopic ratios, 1.02043 and 1.02262, denote an N−O motion with substantial coupling to the metal atom.

A weaker band at 1744.7 cm^{-1} appears to track with the stronger 1693.0 cm^{-1} band on annealing, and both are reduced 50% on photolysis. This band exhibits a ^{15}NO counterpart at 1709.8 cm^{-1} and a triplet with a 1732.6 cm^{-1} middle component with ^{14}NO + ^{15}NO. Note the matching asymmetries in the two triplets indicating interaction between the two central mixed isotopic components.

The 1693.0 and 1744.7 cm^{-1} bands are assigned to the antisymmetric (b_2) and symmetric (a_1) N−O stretching modes in the bent ON−Mn−NO dinitrosyl species, respectively.

The assignments to Mn(NO)$_2$ are strongly supported by the DFT-calculated frequencies presented in Table 5. The stretching modes for this C_{2v} molecule are predicted with observed/calculated ratios 0.990 and 0.997 and excellent agreement between observed and calculated isotopic frequency ratios. These "scale factors" are in accord with those expected for the BP86 functional.[27] The calculations predict weak Mn−N−O deformation modes near 630 cm^{-1} and a stronger Mn−N stretching mode below the range of our instrument.

Mn(NO)$_3$ or Mn−(η^1-NO)$_3$. The dominant band after annealing at 1713.2 cm^{-1} exhibits nitrosyl stretching isotopic ratios (14−16/15−16, 1.01988; 15−16/15−18, 1.02389) as does the associated weaker 1824.1 cm^{-1} band, which maintains constant relative intensity on annealing (14−16/15−16, 1.02019; 15−16/15−18, 1.02335). The mixed 14−16/15−16 spectra in Figure 3 demonstrate that these bands are due to a pyramidal molecule of C_{3v} symmetry. The different quartet patterns for each absorption grow in together on annealing. The approximately 2:1:1:2 relative intensities are characteristic of a doubly degenerate antisymmetric ligand stretching mode where both Mn(^{14}N^{16}O)$_3$ and Mn(^{14}N^{16}O)$_2$(^{15}N^{16}O) contribute to the intense 1713.2 cm^{-1} band and both Mn(^{14}N^{16}O)(^{15}N^{16}O)$_2$ and Mn(^{15}N^{16}O)$_3$ contribute to the strong 1679.8 cm^{-1} band.[29] An analogous quartet was observed at 1679.8, 1663.1, 1651.0, 1640.6 cm^{-1} in the ^{15}N^{16}O/^{15}N^{18}O experiment. The approximately 1:3:3:1 relative intensities for the 1824.1 band system in the ^{14}N^{16}O/^{15}N^{16}O experiment, on the other hand, are characteristic of the nondegenerate symmetric ligand stretching modes of the four isotopic molecules and show the statistical weights of the isotopic molecules present.

The 534.3 cm^{-1} band, also associated by annealing, exhibits different isotopic ratios (14−16/15−16, 1.02819; 15−16/15−18, 1.00864) that are characteristic of a predominately Mn−N stretching mode. The mixed isotopic sextet is due to the doubly

TABLE 6. Isotopic Frequencies (cm^{-1}) and Intensities (km/mol) Calculated (BP86/6-311G*) for $Mn(NO)_3$ in the $^1A''$ State

$(14-16)_3$, ν (I)	$(14-16)_2(15-16)$	$(14-16)(15-16)_2$	$(15-16)_3$	$(15-18)_3$
1849.6(38)	1839.3(67)	1827.0(82)	1810.7(37)	1771.4
1745.9(1199)	1745.9(1196)	1730.7(1139)	1710.3(1149)	1671.4
1745.9(1199)	1719.5(1137)	1710.3(1149)	1710.3(1149)	1671.4
738.7(7)	733.7(7)	728.7(7)	723.7(7)	718.8
675.3(4)	675.0(4)	673.5(4)	670.5(4)	657.5
675.3(4)	672.6(5)	670.8(5)	670.5(4)	657.5
605.5(1)	602.6(1)	599.2(1)	595.9(1)	580.0
586.9(33)	584.5(31)	579.2(31)	570.0(3)	565.3
586.9(33)	577.9(32)	572.0(31)	570.0(31)	565.3
299.0(0.2)	298.4(0.2)	295.8(0.2)	291.6(0.2)	287.1
299.0(0.2)	294.5(0.2)	292.4(0.2)	291.6(0.2)	287.1
277.0(0)	274.5(0)	272.2(0)	270.1(0)	266.0
87.7(0.4)	87.6(0.4)	87.5(0.4)	87.5(0.4)	83.5
87.5(0.7)	87.4(0.8)	87.3(0.8)	87.3(1)	83.4
87.1(4)	87.1(4)	87.0(4)	87.0(3)	83.1

[a] Structure: C_{3v} symmetry, Mn−N = 1.669 Å, N−O = 1.183 Å, ∠Mn−N−O = 165.2°, ∠N−Mn−N = 110.6°.

degenerate Mn−$(NO)_3$ stretching mode. Here, only the Mn-$(^{14}N^{16}O)_3$ molecule contributes to the 534.3 cm^{-1} band, the Mn-$(^{14}N^{16}O)_2(^{15}N^{16}O)$ molecule gives rise to the stronger 532.8 and 526.3 bands, the $Mn(^{14}N^{16}O)(^{15}N^{16}O)_2$ molecule provides the stronger 528.0 and 521.4 cm^{-1} bands, and only the $Mn(^{15}N^{16}O)_3$ molecule absorbs at 519.7 cm^{-1} based on DFT calculation of the mixed isotopic frequencies. The difference in coupling of internal coordinates in the antisymmetric N−O and Mn−N stretching modes is apparent from the mixed isotopic spectrum.

The assignments to pyramidal $Mn(NO)_3$ receive confirmation from the DFT frequency calculations summarized in Table 6. First note that the calculation predicts a very strong antisymmetric ligand vibration at 1745.9 cm^{-1} and a much weaker symmetric counterpart at 1849.6 cm^{-1}, with observed/calculated ratios of 0.981 and 0.986, respectively. The calculated isotopic frequency ratios and mixed isotopic quartet patterns are in excellent agreement with the observed values and spectra. The antisymmetric Mn−N stretching mode predicted at 586.9 cm^{-1} was observed at 534.3 cm^{-1} with a slightly lower observed/calculated ratio (0.910). Again, the calculations predict the observed sextet mixed isotopic pattern and isotopic ratios (14−16/15−16, 1.02979; 15−16/15−18, 1.00835) in excellent agreement with the observed spectrum.

The much weaker degenerate Mn−N−O deformation mode is predicted at 675.4 cm^{-1}, and a sharp 594.1, 591.0 cm^{-1} band pair (observed/calculated = 0.880) appears to track with the 534.3, 539.3 cm^{-1} pair for the degenerate Mn−N stretching mode. The 594.1, 591.0 cm^{-1} bands exhibit isotopic ratios in excellent agreement with values from the isotopic frequencies calculated for the degenerate Mn−N−O deformation mode. The mixed isotopic multiplet is complicated by the extra band, but the stronger central feature at 592.1 cm^{-1} from overlap of two mixed isotopic bands is in accord with the calculations.

The 1728.0 cm^{-1} band is favored at higher Mn levels and on annealing with respect to $Mn(NO)_3$ so a dimanganese species must be considered. The isotopic frequency ratios of the 1728.0 cm^{-1} band again denote a nitrosyl stretching mode, and the quartet pattern suggests a doubly degenerate mode, as described for $Mn(NO)_3$. The sharp weaker 1827.0 cm^{-1} band appears to track with the 1728.0 cm^{-1} band at higher Mn levels on annealing, and it too reveals a quartet pattern much like the 1824.1 cm^{-1} band of $Mn(NO)_3$. In fact, the agreement between isotopic ratios for the 1827.0 and 1824.1 cm^{-1} bands, on one hand, and the 1728.0 and 1713.2 cm^{-1} bands, on the other, is striking. This suggests a $(ON)_3Mn-Mn(NO)_3$ species with a weak Mn−Mn bond where the second $(ON)_3Mn$ species can be considered a fourth ligand for the first $Mn(NO)_3$ complex.

Mn_2NO Molecules. Two other sets of absorptions, the sharp 451.7 cm^{-1} band and the 994.1, 838.8 cm^{-1} pair, are favored at high Mn/NO and disfavored at high NO/Mn ratios. These bands exhibit doublets with mixed $^{14}NO/^{15}NO$, so a single NO submolecule is involved. Furthermore, thermal studies have shown that reactions of diatomic manganese are important,[30] and the Mn_2NO stoichiometry is therefore suggested.

The sharp 451.6 cm^{-1} band has unusual isotopic ratios, 1.01006 and 1.02194, that are less than the diatomic N−O, Mn−N, and Mn−O ratios, so the 451.6 cm^{-1} band is clearly due to a mixed coordinate motion. Hence, the Mn[NO]Mn ring is suggested.

The sharp, weak 994.1 and 838.8 cm^{-1} bands increase together on photolysis and on annealing. They share an unusual relationship: the 994.0 cm^{-1} band exhibits a 14−16/15−16 ratio slightly higher than diatomic Mn−N, and the 838.8 cm^{-1} band has a 15−16/15−18 ratio higher than diatomic MnO. It appears that these bands are terminal N and O vibrations, but the mass partner is heavier than Mn. The 994.0 cm^{-1} band gives a doublet with $^{14}N^{16}O + {}^{15}N^{16}O$ indicating the involvement of a single NO submolecule. These bands are tentatively assigned to NMnMnO.

The sharp 1662.6 cm^{-1} absorption grows on annealing and is decreased by photolysis. The mixed 14/15 spectrum revealed a triplet for two equivalent NO subgroups, and the isotopic ratios are indistinguishable from those of the 1693.0 cm^{-1} band of $Mn(NO)_2$. Calculations predict the strongest band of $Mn(NO)_2^-$ almost 100 cm^{-1} lower. The 1662.6 cm^{-1} band is favored relative to 1693.0 cm^{-1} at higher relative Mn/NO and is absent at the lowest Mn/NO concentration. A tentative assignment to $Mn_2(NO)_2$ is proposed.

Other Absorptions. Since Mn has one more electron than Cr, Mn cannot accommodate four NO ligands in the terminal, nearly linear bonding mode like $Cr(NO)_4$, and $Mn(NO)_3$ is the highest terminal nitrosyl that can be observed here. However, the possibility of another single electron or electron-pair denoting ligand must be considered as $Mn(NO)_3(CO)$ and $(C_6H_5)_3PMn(NO)_3$ have been characterized.[31,32]

It is relevant to compare the photolysis of $Mn(NO)_3(CO)$ in solid argon, which gave rise to a set of new bands at 2105, 1772, 1725, and 1505 cm^{-1} and a pair of new bands at 1714 and 1710 cm^{-1}.[31] The latter pair was suggested to be due to "spectroscopically distinct forms of $Mn(NO)_3$ resulting from minor differences in the local matrix environment." The present assignments and calculations for $Mn(NO)_3$ support this evidence for the photochemical formation of $Mn(NO)_3$. The N−O stretching fundamentals of the C_{3v} $Mn(NO)_3(CO)$ molecule at

1829 and 1742 cm^{-1} are very near the present 1824 and 1713 cm^{-1} values for the C_{3v} $Mn(NO)_3$ molecule, which suggests that the CO ligand has little effect on the structure and bonding in the $Mn(NO)_3$ complex. The former set of bands was assigned to $Mn(CO)(NO)_2(NO^*)$, where NO* denotes a nitrosyl ligand with an altered mode of coordination.[31] Could this be a bent or sideways-bonded NO subunit?

The 1487.1 cm^{-1} band that appears on annealing to 30 K in the experiment using 0.1% NO is in the region of the above nitrosyl with a different structure. The isotopic ratios, 1.01759 and 1.02677, are near the diatomic values, and a doublet was found with isotopic mixtures, so only one NO submolecule is involved. Since $Mn(NO)_3$ cannot accommodate another three-electron-donating nitrosyl, can it accept a truly bent one-electron-donating nitrosyl or a side-on-bonded two-electron-donating NO subgroup?

Similar DFT calculations were done for three possibilities, bent ON-, bent NO-, and sideways [NO] attached to $Mn(NO)_3$. The former two calculations failed to converge, but the latter gave a stable minimum with a sideways [N−O] frequency of 1391.5 cm^{-1} and isotopic ratios 1.0180 and 1.0283. Thus, we tentatively assign the 1487.1 cm^{-1} band to the $Mn(NO)_3(NO^*)$ molecule, where NO* represents a sideways-bonded NO subgroup or $Mn(NO)_3[NO]$. Other absorptions for this molecule may be included in the broad 1766 cm^{-1} band.

This further suggests that the $Mn(CO)(NO)_2(NO^*)$ photochemical product[31] absorbing at 1505 cm^{-1} also involves sideways-bound NO as the alternate mode of bonding. It is interesting to note that this $Mn(CO)(NO)_2(NO^*)$ product has been prepared by annealing argon samples containing Mn, NO, and CO in this laboratory.

A number of other bands in the tables show nitrosyl isotopic ratios, but these bands grow on annealing, and mixed isotopic counterparts cannot be identified in these overlapping spectral regions. These bands are due to aggregate species that remain unidentified.

Finally, bands at 862.3 and 858.3 cm^{-1} just above MnO at 833.1 cm^{-1} show very small nitrogen-15 shifts and oxygen-18 shifts slightly higher than MnO. These bands increase on annealing and are probably due to ligated MnO. Corresponding bands at 1791.5 and 1794.8 cm^{-1} are probably due to the ligand in this (ON)MnO species. Likewise, the sharp 987.8 cm^{-1} band shows a 16/18 ratio near that of OMnO at 948.0 cm^{-1}, and this band is appropriate for $(ON)MnO_2$. The weak 1843.5 cm^{-1} band is due to the nitrosyl vibration associated with this complex.

NReO. The 1052.9 and 901.2 cm^{-1} bands and their associated matrix-split components are produced on deposition of laser-ablated Re and NO. The bands exhibit doublets in mixed isotopic experiments that characterize motions of single N and single O atoms. The isotopic frequency ratios of each band are complementary in that the 1052.9 cm^{-1} band exhibits a large 14−16/15−16 ratio (1.03003), near the ReN value of 1.03215, and a small 15−16/15−18 ratio (1.00304) and the 901.2 cm^{-1} band shows a large 15−16/15−18 ratio (1.05143), near the ReO value of 1.0556, and a small 14−16/15−16 ratio (1.00185). These bands are near the ReN, 1121 cm^{-1}, and ReO, 979 cm^{-1}, fundamental frequencies,[33,34] and assignment to the NReO insertion product follows. The NScO, NTiO, NVO, and NCrO insertion products all exhibit essentially uncoupled M−N and M−O stretching modes,[7,35,36] as does NReO, in contrast to NMnO.

The weak 1038.0 and 860.9 cm^{-1} bands increase 2-fold together on 25 K annealing and are almost destroyed on photolysis, the first in common with NReO but the second in contrast. The isotopic ratios are similar to those of NReO as are the band positions. The photochemical behavior suggests a tentative assignment to $NReO^-$. Although calculations were not done for NReO, note that the calculated frequency relationship between $^3A''$ NMnO and $^4A''$ $NMnO^-$ is the same as for the bands assigned here to NReO and $NReO^-$.

Re[NO] or Re−(η^2-NO). The 1137.2 cm^{-1} band shows N−O stretching isotopic ratios and evidence for a single NO molecule. The evidence is consistent with assignment to the cyclic Re-[NO] species observed at 1236.8 cm^{-1} for Mn[NO] and at 1108.8 cm^{-1} for Cr[NO].[7]

Re−(η^1-NO)$_x$. There is no clear evidence for the mononitrosyl, which is expected to be a weaker absorber than the dinitrosyl. The strong 1651.6 cm^{-1} band that grows on annealing gives rise to the triplet pattern expected for $Re(NO)_2$ and more nearly diatomic N−O isotopic ratios (1.01800, 1.02736) denoting less coupling to the heavier Re atom than that found for $Mn(NO)_2$ (isotopic ratios 1.02033, 1.02262). The 1651.6 cm^{-1} band can be assigned to $Re(NO)_2$ with confidence.

The strong 1677.7 cm^{-1} band also grows on annealing and has the same relationship with the $Re(NO)_2$ absorption that $Mn(NO)_3$ has with $Mn(NO)_2$. Unfortunately the 1677.7 cm^{-1} band is not strong enough to exhibit the intermediate components found for $Mn(NO)_3$. The 1677.7 cm^{-1} band is probably due to $Re(NO)_3$, but the assignment must be considered tentative at this stage.

A number of other absorptions grow on annealing and are due to aggregate species. The most prominent of these, 1684.2 cm^{-1}, might be due to a dimetal species such as $Re_2(NO)_6$, but this identification is only a suggestion.

Reaction Mechanisms. Several comparisons can be made within the present observations. Both η^1 and η^2 compounds are formed with thermal and laser-ablated Mn atoms. This means that little activation energy is required for reactions 1 and 2, which are exothermic by 48.2 and 22.6 kcal/mol, respectively, based on BP86/6-311+G* calculated energies.

$$Mn + NO \rightarrow MnNO\ (\Delta E = -48.2\ \text{kcal/mol}) \quad (1)$$

$$Mn + NO \rightarrow Mn[NO]\ (\Delta E = -22.6\ \text{kcal/mol}) \quad (2)$$

The addition of successive nitrosyl ligands is also exothermic, and these reactions occur on annealing in the argon matrix. Note that the average Mn−NO bond energy increases from 48.2 to 59.7 to 60.7 kcal/mol in the $Mn(NO)_x$, $x = 1-3$ nitrosyls.

$$MnNO + NO \rightarrow Mn(NO)_2\ (\Delta E = -71.2\ \text{kcal/mol}) \quad (3)$$

$$Mn(NO)_2 + NO \rightarrow Mn(NO)_3\ (\Delta E = -62.8\ \text{kcal/mol}) \quad (4)$$

The insertion reaction 5 is even more exothermic, 52.4 kcal/mol, but the bands assigned here to NMnO are not observed with thermal atoms; the molecule is formed with laser-ablated Mn atoms and the bands *increase* on broad-band photolysis but *decrease* on annealing. Hence, activation energy is required for

$$Mn + NO \rightarrow NMnO(\Delta E = -52.4\ \text{kcal/mol}) \quad (5)$$

the insertion reaction, and this activation energy can be provided by the laser-ablation process or by broad-band photolysis. Laser-ablated Mn is rich in ^8P metastable Mn, and these metastable states have a long enough lifetime[37] to reach the matrix and react in the condensing layer before relaxation. A similar mechanism was proposed to account for the Mn insertion reaction with O_2.[12]

The spectra of laser-ablated Mn and Re also reveal some differences. The energy transferred to the condensing sample

is higher for Re than Mn as the yields of NO_2, $(NO_2)^+$, and N_2O_3 are much higher with Re. This is also demonstrated by the observation of ReN at 1117.2 cm^{-1} in the argon matrix and a higher yield of OReO compared to OMnO.[12,36]

The same type of products NReO, $Re(NO)_2$, and Re[NO], were observed as those found for Mn, and the relative yields were, more or less, the same.

Conclusions

Reactions of thermal and laser-ablated Mn atoms with NO produce the Mn−$(\eta^1$-NO$)_x$ complexes ($x = 1-3$) and Mn−$(\eta^2$-NO$)_x$ ($x = 1,2$), but in addition, laser-ablated Mn gives the NMnO insertion product. The $Mn(NO)_2$ complex has C_{2v} symmetry based on isotopic spectra of two N−O stretching modes and DFT calculations of isotopic frequencies. The $Mn(NO)_3$ complex is shown to have C_{3v} symmetry through the observation of mixed isotopic spectra for four vibrational modes including the symmetric (a_1) and antisymmetric (e) N−O ligand stretching modes and DFT calculations of isotopic fundamentals. Laser-ablated Re gave similar products.

Density functional theory (BP86/6-311+G*) has been used to predict isotopic frequencies for three different bond types of Mn/NO species. Although the NScO, NTiO, NVO, and NCrO insertion product vibrational spectra have been characterized extremely well by these DFT calculations,[7,35,36] the mode mixing observed in NMnO is not adequately described by the present calculation although the Mn−N and Mn−O stretching frequencies are observed at 0.91 and 0.94 times the calculated frequencies. This is presumably due to the mixing of other low-lying d-orbital configurations that are not accounted for at the DFT level of theory. On the other hand, the side-bonded Mn-[NO] species is adequately described by a strong mode calculated at 1261.5 cm^{-1} and observed at 1236.8 cm^{-1} and a compatible normal mode description based on very good agreement between calculated and observed isotopic frequency ratios.

The $Mn(NO)_2$ dinitrosyl is extremely well-described by DFT. First, the two dinitrosyl stretching modes are matched between theory and experiment by 0.990 and 0.997 scale factors, which are expected for the BP86 functional.[27] Second, the observed and calculated $Mn(NO)_2$ isotopic frequency ratios as a normal mode description match very well (i.e., antisym N−O 14/15 obsd (1.02043), calcd (1.02069); 16/18 obsd (1.02262), calcd (1.02345).

The $Mn(NO)_3$ assignments are confirmed by DFT calculations. First, the two N−O stretching modes of the C_{3v} complex are predicted with 0.981 and 0.986 scale factors and correct relative intensities, the degenerate Mn−N stretching mode scale factor is 0.91, whereas the Mn−N−O deformation mode scale factor is 0.88. The proof of the problem is in the isotopic frequency ratios, which are well-matched for all four vibrational modes using pure isotopic frequencies. Even the spectra of the lower symmetry $Mn(^{14}N^{16}O)_2(^{15}N^{16}O)$ and $Mn(^{14}N^{16}O)(^{15}N^{16}O)_2$ isotopic molecules are well-described by the DFT calculations.

Clearly, DFT isotopic frequency calculations are an important complement and support for experimental studies of new molecular species.

Acknowledgment. We gratefully acknowledge NSF support under Grant No. CHE 97-00116.

References and Notes

(1) Cotton, F. A.; Wilkinson, G. *Advanced Inorganic Chemistry*, 5th ed.; Wiley-Interscience: New York, 1988.

(2) Herberhold, M.; Razasi, A. *Angew. Chem., Int. Ed. Engl.* **1972**, *11*, 1092. Swanson, B. I.; Satija, S. K. *J. Chem. Soc., Chem. Commun*. **1973**, 40.

(3) Hedberg, L.; Hedberg, K.; Satija, S. K.; Swanson, B. I. *Inorg. Chem.* **1985**, *24*, 2766.

(4) Chiarelli, J. A.; Ball, D. W. *J. Phys. Chem.* **1994**, *98*, 12828.

(5) Ball, D. W.; Chiarelli, J. A. *J. Mol. Struct.* **1995**, *372*, 113.

(6) Ruschel, G. K.; Nemetz, T. M.; Ball, D. W. *J. Mol. Struc*. **1996**, *384*, 101.

(7) Zhou, M. F.; Andrews, L. *J. Phys. Chem. A* **1998**, *102*, 7452.

(8) Blanchet, C.; Duarte, H. A.; Salahub, D. R. *J. Chem. Phys. 1997*, *106*, 8778.

(9) Hassanzadeh, P.; Andrews, L. *J. Phys. Chem*. **1992**, *96*, 9177.

(10) Chertihin, G. V.; Saffel, W.; Yustein, J. T.; Andrews, L.; Neurock, M.; Ricca, A.; Bauschlicher, C. W., Jr. *J. Phys. Chem*. **1996**, *100*, 5261.

(11) Andrews, L.; Bare, W. D.; Chertihin, G. V. *J. Phys. Chem. A* **1997**, *101*, 8417.

(12) Chertihin, G. V.; Andrews, L. *J. Phys. Chem. A* **1997**, *101*, 8547.

(13) Andrews, L.; Zhou, M. F.; Willson, S. P.; Kushto, G. P.; Snis, A.; Panas, I. *J. Chem. Phys*. **1998**, *109*, 177.

(14) Andrews, L.; Zhou, M. F.; Bare, W. D. *J. Phys. Chem. A* **1998**, *102*, 5019.

(15) Worden, D.; Ball, D. W. *J. Phys. Chem.* **1992**, *96*, 7167.

(16) Milligan, D. E.; Jacox, M. E. *J. Chem. Phys*. **1971**, *55*, 3404.

(17) Hacaloglu, J.; Suzer, S.; Andrews, L. *J. Phys. Chem*. 1990, *94*, 1759. Strobel, A.; Knoblauch, N.; Agreiter, J.; Smith, A. M.; Nerder-Schatteburg, G.; Bondybey, V. E. *J. Phys. Chem*. **1995**, *99*, 872.

(18) Frisch, M. J.; Trucks, G. W.; Schlegel, H. B.; Gill, P. M. W.; Johnson, B. G.; Robb, M. A.; Cheeseman, J. R.; Keith, T.; Petersson, G. A.; Montgomery, J. A.; Raghavachari, K.; Al-Laham, M. A.; Zakrzewski, V. G.; Ortiz, J. V.; Foresman, J. B.; Cioslowski, J.; Stefanov, B. B.; Nanayakkara, A.; Challacombe, M.; Peng, C. Y.; Ayala, P. Y.; Chen, W.; Wong, M. W.; Andres, J. L.; Replogle, E. S.; Gomperts, R.; Martin, R. L.; Fox, D. J.; Binkley, J. S.; Defrees, D. J.; Baker, J.; Stewart, J. P.; Head-Gordon, M.; Gonzalez, C.; Pople J. A. *Gaussian 94*, revision B.1; Gaussian, Inc.: Pittsburgh, PA, 1995.

(19) Perdew, J. P. *Phys. Rev. B* **1986**, *33*, 8822.

(20) Becke, A. D. *J. Chem. Phys*. **1993**, *98*, 5648.

(21) McLean, A. D.; Chandler, G. S. *J. Chem. Phys.* **1980**, *72*, 5639.

(22) Krishnan, R.; Binkley, J. S.; Seeger, R.; Pople, J. A. *J. Chem. Phys.* **1980**, *72*, 650.

(23) Wachters, A. J. H. *J. Chem. Phys.* **1970**, *52*, 1033. Hay, P. J. *J. Chem. Phys.* **1977**, *66*, 4377.

(24) Chertihin, G. V.; Andrews, L.; Rosi, M.; Bauschlicher, C. W., Jr. *J. Phys. Chem. A* **1997**, *101*, 9085. Chertihin, G. V.; Andrews, L.; Bauschlicher, C. W., Jr. *J. Am. Chem. Soc*. **1998**, *120*, 3205.

(25) Lanzisera, D. V.; Andrews, L. *J. Am. Chem. Soc.* **1997**, *119*, 6392.

(26) Bauschlicher, C. W., Jr. *Chem. Phys. Lett.* **1995**, *246*, 40.

(27) Scott, A. P.; Radom, L. *J. Phys. Chem*. **1996**, *100*, 16502.

(28) Jonas, V.; Thiel, W. *J. Chem. Phys.* **1996**, *105*, 3636.

(29) Darling, J. H.; Ogden, J. S. *J. Chem. Soc., Dalton Trans*. **1972**, 2496.

(30) Huber, H.; Kundig, E. P.; Ozin, G. A.; Poe, A. J. *J. Am. Chem. Soc.* **1975**, *97*, 308.

(31) Crichton, O.; Rest, A. J. *J. Chem. Soc., Dalton Trans.* **1977**, 202.

(32) Wilson, R. D.; Bau, R. *J. Organomet. Chem.* **1980**, *191*, 123.

(33) Balfour, W. J.; Ram, R. S. *J. Mol. Spectrosc.* **1983**, *100*, 164.

(34) Ram, R. S.; Bernath, P. F.; Balfour, W. J.; Cao, J.; Qian, C. X. W.; Rixon, S. J. *J. Mol. Spectrosc.* **1994**, *168*, 350.

(35) Kushto, G. P.; Zhou, M. F.; Andrews, L.; Bauschlicher, C. W., Jr. Submitted for publication.

(36) Zhou, M. F.; Andrews, L. *J. Phys. Chem. A*, in press.

(37) Levy, M. R. *J. Phys. Chem.* **1989**, *93*, 5195.